Biomimetic and Environmentally Friendly Self-Assembly Behavior of Melamine onto the Surface of Black Phosphorus Nanosheets: Constructing Advanced P/N-Containing Nano Flame Retardants

Wei Cai [a,1], Weiyi Xing [a,1], Tianyang Cui [a], Junling Wang [b], Bicheng Lin [a], Zhaoxin Li [a], Liangyuan Qi [a], Xin Hu [c], Yang Ming [c], Peng Xiao [e], Fuli Bian [a,d], Bin Fei [c], Yuan Hu [a]*

[a]State Key Laboratory of Fire Science, University of Science and Technology of China, Hefei 230026, PR China

[b]Jiangsu Key Laboratory of Hazardous Chemicals Safety and Control, College of Safety Science and Engineering, Nanjing Tech University, Nanjing 211816, China

[c]Institute of Textiles and Clothing, The Hong Kong Polytechnic University, 999077, Hong Kong S.A.R, China

[d]Shanghai Fire Research Institute of Ministry of Emergency Management of China, 601 Zhongshan South 2nd Road, Xuhui District, Shanghai 200032, PR China

[e]State Grid Jiangsu Electric Power Co., Ltd. Research Institute, Nanjing, 211103, Jiangsu, P. R. China

* Corresponding author

E-mail: bianfuli@shfri.cn

[1] These authors contributed equally to this work.

Abstract: Herein, inspired by the hierarchical structure within the biological protein, we adjust the temperature of the aqueous solution to control the unfolding and reconstitution of hydrogen bonds among melamine (MA) molecules, thus preparing

MA-functionalized black phosphorus (MA@BP) nanosheets. As confirmed by the first-principles calculations, melamine can spontaneously adsorb onto the surface of BP nanosheets and enhance the interfacial interactions between BP nanosheets and thermoplastic polyurethane (TPU) matrix. Compared to pure BP nanosheets, MA@BP nanosheets present more efficient suppression effects in heat release and toxic CO production. Besides, due to the photo-thermal conversion effect of BP nanosheets, TPU-MA@BP-2.0 presents an equilibrium temperature of ~80 ºC under simulated sunlight of 1.0 kW/m^2 and a significant solar de-icing performance. The solve-free and hydrogen-bond assembly method not only solves the lack problem of functional groups for the functionalization of BP nanosheets, but also develops a flame-retardant and photo-thermal polymer nanocomposite applied in various occasions.

Keywords: A. Multifunctional composites; A. Polymer-matrix composites (PMCs); B. Flame/fire retardancy; B. Thermal properties

1. Introduction

Polymer materials have become a huge consumable in society today and applied recently in wide fields, due to their high mechanical property, lightweight, and resistance to environment/acid/base. Among them, thermoplastic polyurethane is particularly popular as it can be used in coating, leather, binder, flexible tubes, and so on[1]. Recently, for safeguarding the durability of outdoor facilities, polyurethane resin is usually used as the coating material to enhance the resistance to environmental corrosion. However, outdoor facilities will frequently encounter fire and icing issues caused by inappropriate working conditions and terrible weather. For example, a large amount of ice will accumulate on the surface of the wind turbine blade located in high altitude area, significantly increasing the blade weight to cause the turbine overload. Meanwhile, the overload working condition easily leads to a fire accident. The same problem is also faced by the electrical cable, which will collapse under heavy snows and further give rise to a fire. Unfortunately, used as coating materials, thermoplastic polyurethane, mainly composed of carbon, oxygen, and nitrogen, is easy to be ignited

at high temperatures [2]. During the combustion, a lot of heat, toxic gas, and smoke particles will be released to threaten the security of lives and property of the people. Solutions to overcome the fire hazards have been found that include adding flame retardants or modifying the chain structure of TPU with flame-retardant elements or groups. Even though the flame-retardant modification of chain structure is highly efficient and has few side effects, this achievement usually involves the production craft of polymer resin which causes a huge increase in commercial cost. In addition, the direct application of PU-based materials as the coating materials of outdoor facilities does not solve the icing hazards[3].

As reported by previous literature, the incorporation of two-dimensional nanomaterials (e.g., graphene, MoS_2, boron nitride, and so on) in polymer resin is a simple but highly efficient approach to improve the fire safety and other performances of polymer materials[4]. Due to the thermally stable layer structure, two-dimensional nanomaterials can present a barrier and labyrinth effect to suppress the delivery between heat and pyrolysis products, during polymer combustion. For example, Huang et al. prepared P/N-containing graphene-based nano flame retardants, with a simple two-step method[5]. The peak heat release rate and peak smoke production rate of the acrylonitrile-butadiene-styrene copolymer are respectively reduced by 51% and 60% with the incorporation of 1.0 wt% graphene-based nano flame retardants. Due to its high electrical conductivity, graphene is not applicable to electronic packaging materials[6]. Therefore, researchers have started to focus on the alternative of graphene nanosheets, including MoS_2 and boron nitride. In addition, the single function based on layer structure also limits the flame retardancy improvement of polymer materials.

Recently, BP and MXene have emerged as the two most promising nano flame retardants, presenting their respective merits[7, 8]. With respect to MXene nanosheets, BP nanosheets with lower electrical conductivity are more applicable to electronic packaging materials[9]. In addition, the full P element characteristic imparts BP nanosheets with extremely excellent flame retardancy. As reported by Hu et al., the addition of pure BP nanosheets in unsaturated polyester leads to a reduction of 42.7% and 21.0% in PHRR and THR[10]. A similar suppression effect of pure BP nanosheets

in the fire hazards of TPU materials is also reported[11]. However, even though BP nanosheets have both layer structure and flame retardant elements, the single phosphorus element does not present synergistic flame retardancy[12]. Meanwhile, the lack of functional groups in the pure BP nanosheets also limits the further modification of BP nanosheets.

Due to its high nitrogen content, melamine has been also used as an environmentally friendly flame retardant [13]. After being protonated by hydrochloric acid or acetic acid, positively charged melamine is usually employed to react with phytic acid and phosphoric acid to synthesize P/N-containing flame retardants[13, 14]. It is an interesting phenomenon that melamine is hard to dissolve in a water solution, even with a lot of amino groups[15]. It is because the hydrogen-bond interaction is preferred among melamine molecules, rather than between melamine and water. In nature, biological protein materials feature multiscale hierarchical structures composed primarily of hierarchical assemblies of hydrogen bonds (Figure 1a)[16, 17]. A representative example is spider silk, which has highly well-organized and hydrogen-bond assembled β-sheet nano-crystals that can significantly enhance the comprehensive mechanical[18]. Therefore, it is speculated that independent melamine at the molecule level can be assembled into an ordered nanostructure with hydrogen-bond interaction[19, 20].

Herein, inspired by the hierarchical structure within biological protein composed of hydrogen-bond interaction, we develop an environmentally friendly approach to prepare melamine-functionalized BP nanosheets that are used as a P/N-containing nano flame retardant (Figure 1b). By adjusting the temperature of the aqueous solution, the hydrogen-bond interaction among melamine molecules is first unfolded and destroyed at high temperatures. Then, BP nanosheets are used as rigid templates and melamine molecules are assembled again with hydrogen-bond interaction, during the cooling process. In addition to water, there are no solvents. Meanwhile, this method does not need to introduce other functional groups onto the surface of BP nanosheets. Obviously, the overall functionalization process is simple and environmentally friendly. In addition, melamine-functionalized BP nanosheets present a synergistic flame retardancy effect

in improving the fire safety of polymer resin.

2. Experimental part

2.1 Materials

Thermoplastic polyurethane (67E85) was supplied by Bangtai Materials Co., Ltd. (China). Melamine (AP) and N,N-dimethylformamide (DMF) were purchased from Sinopharm Chemical Co. Ltd. (China). The bulk black phosphorus is prepared, according to our previous literature[21]. These reagents are used directly, without any purification.

2.2 Preparation of MA@BP nanosheets

Bulk BP crystal of 2.0g was firstly ground into powder and then added to 1000 mL DMF with sonication of 2h. The exfoliated BP nanosheets were collected by centrifugation at 1200 rpm for 10 min. 1.0g melamine was added to 100 mL water at 100 ºC. Until the melamine was completely dissolved, 1.0g BP nanosheets re-dispersed in water were slowly added to the melamine solution at 100 ºC. After the addition of BP nanosheets solution, the mixed system was slowly cooled to room temperature. Finally, the products were collected by vacuum filtration and freeze-dried.

2.3 Preparation of TPU-MA@BP composite

Before processing, TPU was dried in an oven at 100 ºC for 24 h to remove water. TPU-based composites were prepared by solvent blending and co-coagulation. Typically, 0.5 g MA@BP was dispersed in 100 mL DMF with sonication for 1 h. Subsequently, 49.5 g TPU dissolved in DMF was introduced into MA@BP dispersion and stirred for 2 h. Finally, the above solution was poured into 1 L of deionized water with a slight stirring. The flocculate obtained was collected through vacuum filtration and dried in a 100 ºC oven for 12 h to remove solvent. The sample was hot-pressed at 180 ºC and 10 MPa for 10 min into sheets with the appropriate size. Other samples were prepared with the same procedure.

2.4 Measurements and Characterization

X-ray diffraction (XRD) patterns were obtained with a Japan Rigaku D/Max-Ra rotating anode X-ray diffractometer equipped with a CuKα tube and Ni filter (λ =

0.1542 nm). The structure and features of the char residue were observed with an XL-30 ESEM scanning electron microscope (SEM) at an acceleration voltage of 20.0 kV. Transmission electron microscopy (TEM) was used to observe the nanostructure morphology with a JEOL JEM-2100F transmission electron microscope at an accelerating voltage of 200 kV. Thermogravimetric analysis (TGA) was executed with a TGA Q5000 IR thermogravimetric analyzer (TA Instruments, U.S.) at a heating rate of 20 ºC/min. Thermogravimetric analysis-infrared spectrometry (TG-IR) was investigated with a TGA Q5000IR thermogravimetric analyzer linked to a Nicolet 6700 FTIR spectrophotometer from 20 to 700 ºC at 10 ºC/min (N_2 atmosphere, flow rate of 30 mL/min). A combustion test was carried out on a cone calorimeter (Fire Testing Technology, UK) according to ISO 5660 standard procedures, with 100 × 100 × 3 mm^3 specimens. Each specimen was exposed horizontally to a 35 kW/m2 external heat flux. X-ray photoelectron spectroscopy (XPS) was performed to characterize the element of graphene with a VG ESCALB MK-II electron spectrometer. The excitation source was an Al Kα line at 1486.6 eV.

2.5 Photo-thermal conversion and de-icing test

The photo-thermal conversion effect was analyzed by an IR camera (HIKMICRO E09), a thermoelectric couple, and a Xe lamp (CELPE300L-3A). With simulated sunlight of 1.0 kW/m^2 provided by a Xe lamp, the surface temperature was recorded by the IR camera and thermoelectric couple. A homemade measurement system mainly consisting of cold hydrazine with a diameter of 35.0 cm and a height of 50.0 cm, a Xe lamp (CELPE300L-3A), an IR camera (HIKMICRO E09), and a digital camera (FDRAX700 4K) was used to conduct the solar de-icing experiments. A water drop was frozen onto the surface of pure TPU and its composites. After being radiated by simulated solar light of 1.0 kW/m^2, the melt and slide behavior of ice pellets located on the surface of pure TPU and its composites were recorded to evaluate the solar de-icing performance. The humidity of the anti-icing test ranged from 70% to 80%. Meanwhile, the test pressure is 101.325 kPa, i.e., standard atmospheric pressure.

3. Results and Discussion

3.1 Adsorption Energy Calculation

During the cooling process, melamine molecules will be precipitated spontaneously and may form a hydrogen-bond crosslinking product. Using BP nanosheets as a template, the self-assembly behavior driven by the hydrogen bond probably happens on the surface of BP nanosheets. Meanwhile, the existence of melamine will enhance the interfacial interaction between BP nanosheets and TPU matrix. For demonstrating the feasibility, the adsorption energy of the different systems will be calculated by density functional theory (DFT) based on the first principles. The adsorption energy is calculated by the following equation (1, 2, and 3):

$$E_{ads(MA@BP)}=E_{(MA@BP)}-E_{MA}-E_{BP} \quad (1)$$

$$E_{ads(TPU/BP)}=E_{(TPU/BP)}-E_{TPU}-E_{BP} \quad (2)$$

$$E_{ads(TPU/MA@BP)}=E_{(TPU/MA@BP)}-E_{TPU}-E_{MA@BP} \quad (3)$$

where $E_{ads(MA@BP)}$, $E_{ads(TPU/BP)}$ and $E_{ads(TPU/MA@BP)}$ are the adsorption energy of MA@BP, TPU/BP, and TPU/MA@BP systems, respectively. Meanwhile, $E_{(TPU/MA@BP)}$, $E_{(TPU/BP)}$, $E_{(MA@BP)}$, E_{MA}, and E_{BP} are the corresponding energy. To decrease the computational effort, simplified model structures with the most stable configuration were employed (Figure 1c). The energy of TPU/MA@BP, TPU/BP, MA@BP, BP, TPU, and MA are -8371.07, -7924.30, -7274.15, -6827.41, -1096.88, and -446.56 hartree, respectively. Based on formulas 1, 2, and 3, the $E_{ads(MA@BP)}$, $E_{ads(TPU/BP)}$ and $E_{ads(TPU/MA@BP)}$ are -0.184, -0.010, and -0.204 hartree (Figure 1c). Meanwhile, 1 hartree is equal to 27.211 eV. Therefore, the $E_{ads(MA@BP)}$, $E_{ads(TPU/BP)}$ and $E_{ads(TPU/MA@BP)}$ are -5.007, -0.272, and -5.551 eV. The adsorption energy of up to -5.007 eV indicates that the self-assembly process of melamine will most likely happen on the surface of BP nanosheets. Compared to the TPU/BP system, the absolute value of adsorption energy of TPU/MA@BP system is increased to 5.551 eV from 5.007 eV. In other words, the introduction of melamine is able to enhance the interfacial interaction between BP nanosheets and TPU matrix.

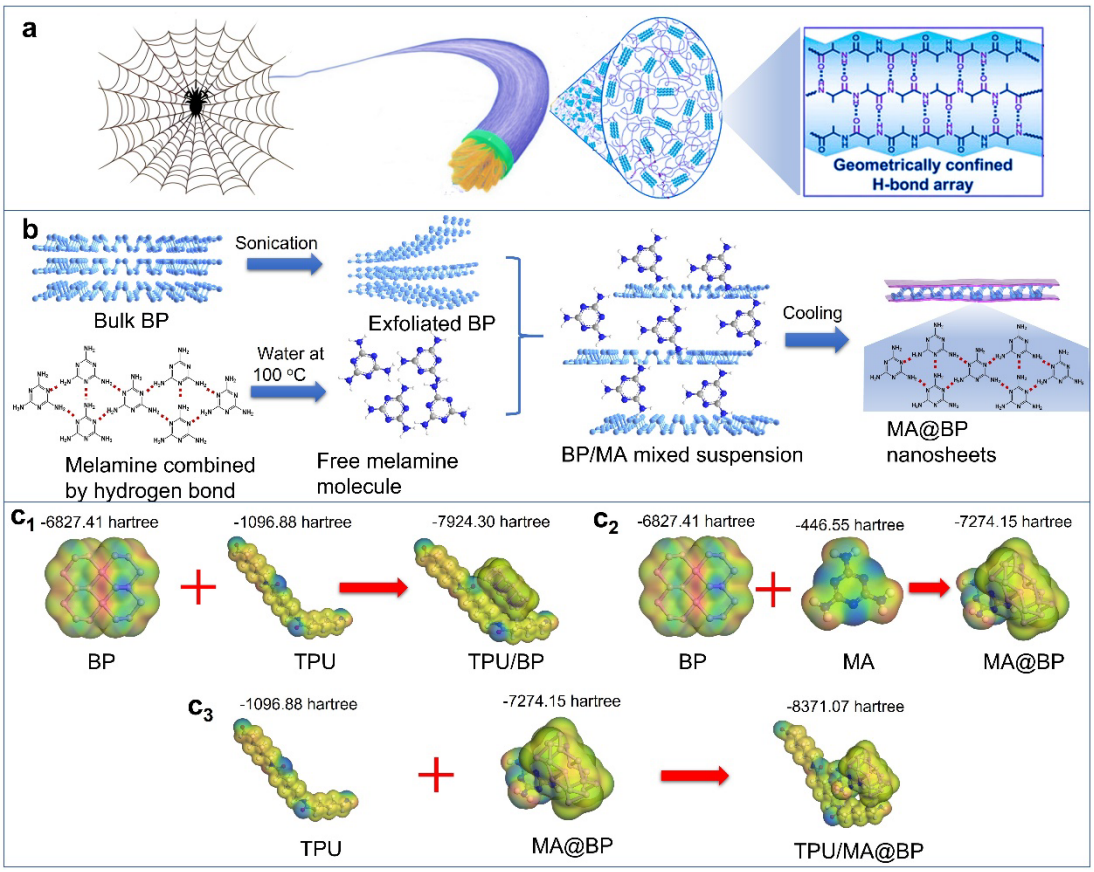

Figure 1 (a) Schematic for the hydrogen-bond interactions within the spider silk; (b) Schematic for the preparation of MA@BP nanosheets; (c) The calculation result of adsorption energy.

3.2. Characteristic of MA@BP nanosheets

By the deposition of melamine, the surface morphology of BP nanosheets will be obviously changed. Based on the SEM photograph, the microstructure of BP nanosheets and MA@BP nanosheets are directly observed (Figure 2). It is found that the surface of pure BP nanosheets is extremely smooth, only with a slightly folded structure (Figure 2a_1). Few protuberances or rough morphology are observed. This phenomenon indicates that pure BP nanosheets prepared by the sonication in liquid can keep their well crystal structure[22]. After being modified by melamine, the surface of MA@BP nanosheets starts to become rough and presents a wave-like structure, which can be attributed to the modification of melamine (Figure 2a_2). The bending and non-straight layer edges demonstrate that the layer and crystal structure of BP nanosheets are

destroyed in a certain degree. As presented in previous literature, BP nanosheets will be degraded easily by the water/oxygen-containing environment[23]. Therefore, the functionalization process inevitably destroys the crystal structure of BP nanosheets. The surface morphology of MA@BP nanosheets is further investigated by TEM photographs. The rough features are uniformly dispersed onto the surface of MA@BP nanosheets, without an ordered structure, indicating amorphous crystal phases (Figures $2b_1$ and $2b_2$). The uniform dispersion indicates that there is not special site for the interactions between melamine and BP nanosheets. The self-assembly process of melamine randomly happens on the surface of BP nanosheets used as rigid templates. The element dispersion and ratio of MA@BP nanosheets are also revealed by SEM-EDS Mapping (Figures 2c, S1, S2, and Table S1). In the SEM EDS spectrum, C, O, N, and P are successfully detected (Figure S1). Obviously, the distribution of P element is completely same as the profile of MA@BP nanosheets (Figure 2c). Compared to the clear comparison of P element, the edge of C and N elements between MA@BP and substance is vaguer (Figures 2c and S2). This phenomenon is attributed to the wide existence of C and N elements in the environment. Fortunately, blank areas of C and N elements are still presented between MA@BP and substance, especially for N element. This result strongly confirms the uniform deposition of melamine onto the surface of MA@BP nanosheets, attributed to the biomimetic self-assembly process. In fact, the mass ratio of C, N, and O provided by the SEM-EDS cannot be used to quantitatively compare the modification amount of melamine. However, the phosphorus content of up to 71.5 wt% indicates that the main composition of MA@BP nanosheets is still BP nanosheets (Table S1).

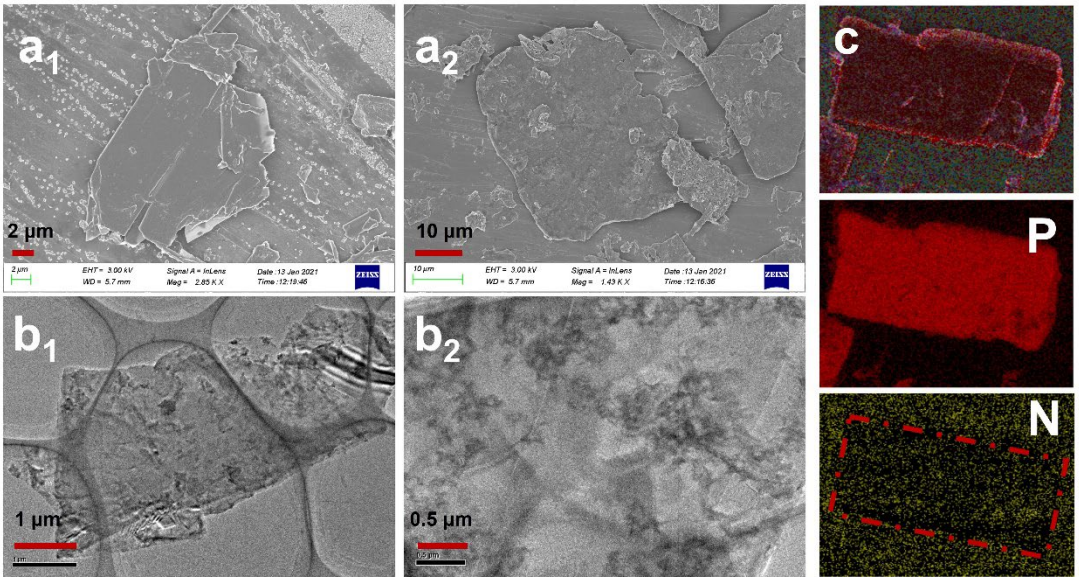

Figure 2 SEM photographs of pure BP (a_1) and MA@BP nanosheets (a_2); (b_1 and b_2) TEM photographs of MA@BP nanosheets in different resolutions; (c) SEM Mapping spectra of phosphorus and nitrogen elements of MA@BP nanosheets;

Due to the modification of melamine, the chemical bond and composition of functionalized BP nanosheets have been significantly changed compared with pure BP. FTIR spectrum can present corresponding details for the change of chemical bonds with the characteristic response (Figure 3a). It is found that pure BP shows characteristic peaks of P=O and PO_3^{4-} near 1175 cm^{-1} and 1021 cm^{-1}[24]. Obviously, even with the smooth surface and straight edge, few oxygen-containing bonds still exist in pure BP nanosheets. The FTIR spectrum of melamine is also studied. The characteristic peaks located in 3467, 3421, 1437, and 812 cm^{-1} are due to the stretch vibration of $-NH_2$. In addition, the vibration of C=N and C-H bonds correspond to characteristic peaks of 1553 and 3130 cm^{-1}[25]. Other characteristic peaks, such as N-N and N=N are shown in 3337 cm^{-1} and 1653 cm^{-1}. It is found that MA@BP nanosheets present the same characteristic peaks as melamine, without the demonstration of P=O and PO_4^{3-} bonds. This result is due to the overlap of characteristic peaks of melamine over the BP nanosheets. The Raman spectra of pure BP and MA@BP in the 200-700 cm^{-1} are presented in Figure 3b. Three characteristic peaks near 362, 437, and 467 cm^{-1} are corresponding to out-of-plane (A_g^1) and in-plane phonon modes (A_g^2 and B_{2g}), respectively[26]. In detail, the characteristic peaks of A_g^1, A_g^2, and B_{2g} modes of pure

BP nanosheets are located in 362.2, 437.8, and 466.3 cm^{-1}, while corresponding peaks in MA@BP nanosheets are in 361.4, 437.7, 466.1 cm^{-1}. Compared to pure BP nanosheets, A_g^1, A_g^2, and B_{2g} modes in MA@BP nanosheets move to the lower wavenumber, implying the potential interaction between melamine and BP nanosheets[27].

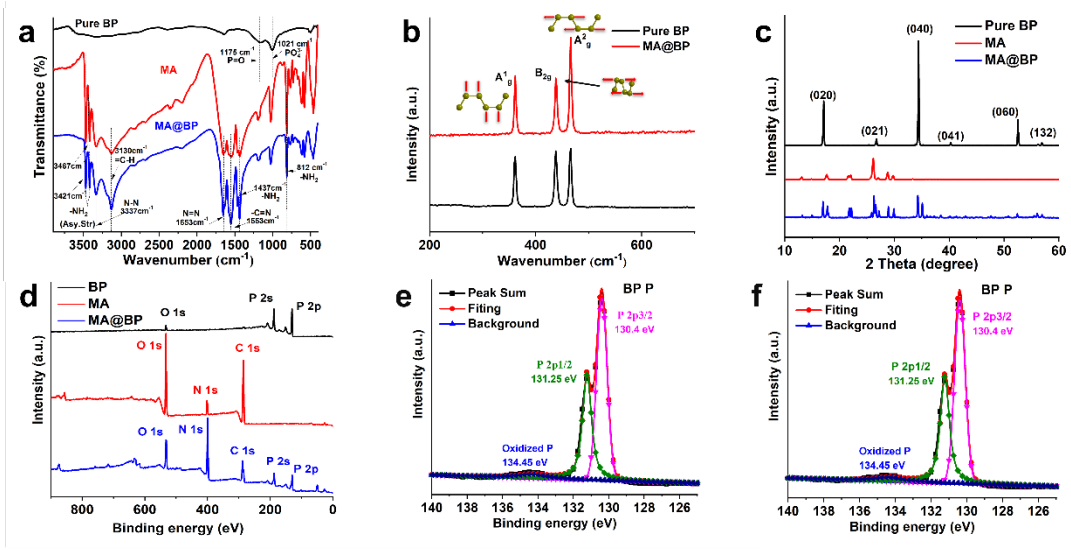

Figure 3 FTIR (a), Raman (b), XRD (c), and XPS (d) spectra of pure BP and MA@BP nanosheets; high-resolution XPS spectra of P in pure BP (e) and MA@BP (f) nanosheets.

XRD spectrum is also performed to investigate the crystalline phase of pure BP and MA@BP nanosheets (Figure 3c). Presented by XRD curve of pure BP, high-intensity diffraction peaks at 16.9, 34.4, and 52.7 are corresponding to the (020), (040), and (060) planes of BP crystal[28]. Meanwhile, low diffraction peaks attributed to the (021), (041), and (132) planes are also presented. It is found that, after being modified by melamine, MA@BP still presents obvious diffraction peaks which are at same position with pure BP nanosheets. Other new peaks are attributed to melamine, as shown by the XRD curves of MA and MA@BP nanosheets[29]. The diffraction peaks originating from melamine indicate that an ordered structure is formed during the hydrogen-bond self-assembly process. XPS analysis is carried out to give a more precise element content (Figure 3d). It is found that pure BP nanosheets present an extremely high intensity in P element. Therefore, the appearance of high-intensity oxygen and carbon peaks in

MA@BP nanosheets is attributed to the modification of melamine. The mass percentages of O, P, N, and C elements in MA@BP nanosheets are 15.9 wt%, 19.8 wt%, 38.2 wt%, 26.2 wt%. The investigation depth of XPS analysis is usually lower than 10 nm. Therefore, in view of the structure of MA@BP nanosheets, the N content is overestimated. The high-resolution XPS spectrum of P 2p of pure BP and MA@BP nanosheets is also compared to reveal the oxidation degree (Figures 3e and 3f). Three characteristic peaks at 130.40 131.25, and 134.45 eV correspond to P $2p^{3/2}$, P $2p^{1/2}$, and oxidized P[30]. The ratio value of peak area in high-resolution P 2p XPS spectrum was used to investigate the oxidation degree. The area ratios of P $2p^{3/2}$, P $2p^{1/2}$, and oxidized P are 60.2%, 33.0%, and 6.8%, respectively. After being functionalized by melamine, the corresponding ratio value changed to 47.9%, 22.1%, and 30.0%. This higher ratio for oxidized P means more defect structure. Therefore, based on the above analyses, two conclusions can be obtained: (1) the gradual cooling process from 100 ºC will inevitably destroy the crystal structure of BP nanosheets; (2) melamine molecules will form an ordered structure with hydrogen-bond interactions onto the surface of BP nanosheets.

3.2 Thermal stability of TPU-MA@BP composites

As presented in Figure 4, the TGA curves of pure TPU and TPU/BP composites are also investigated, in a nitrogen atmosphere. It is found that TPU and its composites present a two-step thermal pyrolysis process (Figure 4a). The first and second stages correspond to the degradation in the main chain and pyrolysis of polyols and isocyanates[31]. The addition of pure BP and MA@BP nanosheets will decrease the initial pyrolysis temperature corresponding to a weight loss of 5 wt% ($T_{5wt\%}$). As shown in Figure 4b and Table 1, compared to $T_{5wt\%}$ in pure TPU (304.2 ºC), the slight increase (308.6 ºC) in TPU-MA@BP-0.5 may be due to a reasonable error. With the increasing addition of MA@BP nanosheets, the $T_{5wt\%}$ of TPU-MA@BP-1.0, TPU-MA@BP-1.5, and TPU-MA@BP-2.0 composites gradually decrease to 296.0 ºC, 291.0 ºC, and 290.6 ºC. Meanwhile, incorporated 2.0wt% BP nanosheets lead to 292.6 ºC for T5.0wt% for TPU-BP-2.0. This decreased phenomenon in $T_{5wt\%}$ is also reported in previous literature.

However, based on our previous research works, the thermal degradation temperature in BP nanosheets is obviously higher than 350 ºC, whether in air or nitrogen atmosphere[11]. Therefore, the decreased $T_{5wt\%}$ is not caused by the pyrolysis of BP nanosheets. As demonstrated in the XPS test, there are a lot of phosphoric groups in BP nanosheets. In other words, it is the existence of phosphoric groups which decrease the initial thermal pyrolysis temperature.

As presented in Figure 4c, the incorporated BP and MA@BP nanosheets contributed to the formation of char residue at 800 ºC. For example, the addition of 0.5wt% MA@BP nanosheets increases the char residue at 800 ºC of TPU resin to 6.81 wt% from 4.71 wt%, obviously higher than the additional amount. A gradual increase trend in the char residue at 800 ºC is demonstrated in TPU-MA@BP-0.5, TPU-MA@BP-1.0, and TPU-MA@BP-1.5. However, with 2.0wt% MA@BP nanosheets, the char residue at 800 ºC in TPU-MA@BP-2.0 (8.83 wt%) is less than those of TPU-MA@BP-1.5 (9.56wt%) and TPU-BP-2.0 (9.46wt%). DTG curves are analyzed to reveal the mass loss rate in the thermal pyrolysis process (Figure 4d). As demonstrated by Figure 4e, the peaks corresponding to the first-step thermal pyrolysis are obviously advanced, from 350.5 ºC (pure TPU) to 311.9 ºC (TPU-MA@BP-2.0). This result is consistent with the phenomenon of $T_{5.0wt\%}$. Due to the influences of pure BP and MA@BP nanosheets in $T_{5wt\%}$, a regular trend is not found in the mass loss rate of the first-step pyrolysis ($MLR_{max,1}$). However, $MLR_{max,2}$ with stronger regularity is presented in Figure 4f. In addition to TPU-MA@BP-0.5, the $MLR_{max,2}$ of TPU-MA@BP-1.0, TPU-MA@BP-1.5, and TPU-MA@BP-2.0 are decreased to 0.0666 %/ºC, 0.564 %/ºC, and 0.353%/ºC, compared with pure TPU. Based on the above analyses, it is concluded that the addition of pure BP and MA@BP nanosheets will decrease the initial pyrolysis temperature, attributed to the existence of a phosphoric group. Meanwhile, pure BP and MA@BP nanosheets can increase the formation of char residue at 800 ºC, contributing to the condensed flame retardant mechanism. Besides, the mass loss rate in the second step will be effectively suppressed by the incorporated pure BP and MA@BP nanosheets.

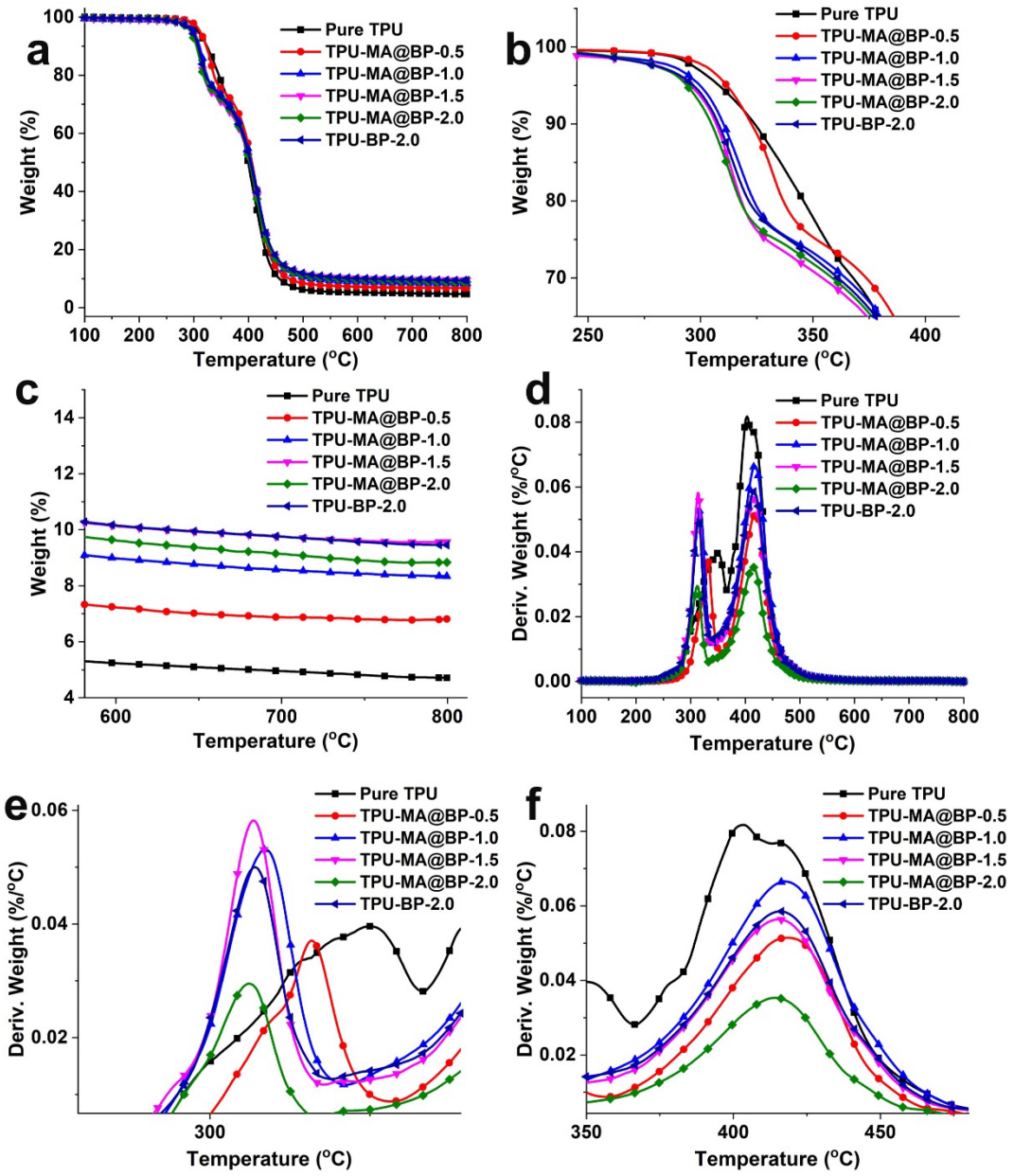

341

342 **Figure 4** TGA (a, b, and c) and DTG (d, e, f) curves of pure TPU and its nanocomposites

343 under nitrogen atmosphere.

344 **Table 1** TGA data of pure TPU and its composites

	$T_{5wt\%}$ (°C)	$MLR_{max,1}$ (%/°C)	$MLR_{max,2}$ (%/°C)	Char residue at 800 °C (wt%)
Pure TPU	304.2	0.0397	0.0817	4.71
TPU-MA@BP-0.5	308.6	0.0371	0.0516	6.81
TPU-MA@BP-1.0	296.0	0.0533	0.0666	8.34
TPU-MA@BP-1.5	291.0	0.0581	0.0564	9.56
TPU-MA@BP-2.0	290.6	0.0296	0.0353	8.83
TPU-BP-2.0	292.6	0.0501	0.0583	9.46

3.3 Fire safety of TPU-MA@BP composites

At present, the cone calorimeter test is regarded as an effective tool for evaluating the fire hazards of polymer composites, in terms of heat release and smoke production[32]. In Figure 5a, the heat release rate versus the time of pure TPU and its composites is recorded during the combustion. It is observed that pure TPU presents a two-step heat release process, turning at ~100s. This phenomenon is similar to the TGA curves, and may be due to the pyrolysis process of the main chain and pyrolysis of polyols and isocyanates. It is found that the addition of pure BP and MA@BP nanosheets will change and advance the turning point (signed by red frame), also corresponding to the first-step thermal pyrolysis of TGA results. The detailed data of peak values of heat release rate (PHRR), total heat release (THR), smoke production rate (SPR), and total smoke release (TSR) are presented in Table 2. Compared to the high PHRR value of pure TPU (982.1 kW/m^2), incorporated 0.5 wt%, 1.0 wt%, 1.5 wt%, and 2.0 wt% MA@BP nanosheets decrease the PHRR values to 836.0 kW/m^2, 800.5 kW/m^2, 683.5 kW/m^2, and 660.6 kW/m^2, respectively. The reduction of up to 32.7% in PHRR of TPU-MA@BP-2.0 confirms the enhancement of fire safety. The incorporation of 2.0 wt% pure BP also leads to a PHRR of 703.0 kW/m^2 in TPU-BP-2.0, higher than that of TPU-MA@BP-2.0. This result indicates that MA@BP nanosheets are more efficient than pure BP nanosheets in fire safety improvement. Meanwhile, THR values of pure TPU, TPU-MA@BP-0.5, TPU-MA@BP-1.0, TPU-MA@BP-1.5, and TPU-MA@BP-2.0 are 61.4 MJ/m^2, 59.4 MJ/m^2, 50.0 MJ/m^2, 48.7 MJ/m^2, and 47.4 MJ/m^2 (Figure 5b). At the same addition amount, 2.0wt% BP nanosheets only decrease the THR of TPU composite to 50.0 MJ/m^2. According to a previous research work, TPU added with 2.0 wt% graphene decorated with bromine and nano-Sb_2O_3 showed a reduction of 8% in THR[33]; in another study reported by our group, TPU incorporated with 2.0 wt% flame retardant functionalized graphene had a THR of lower than 19%[34]. However, in this work, THR of TPU-MA@BP-2.0 is decreased by 22.8%. Such reductions in PHRR and THR together confirm the suppression of MA@BP nanosheets in the heat release behavior of TPU composites.

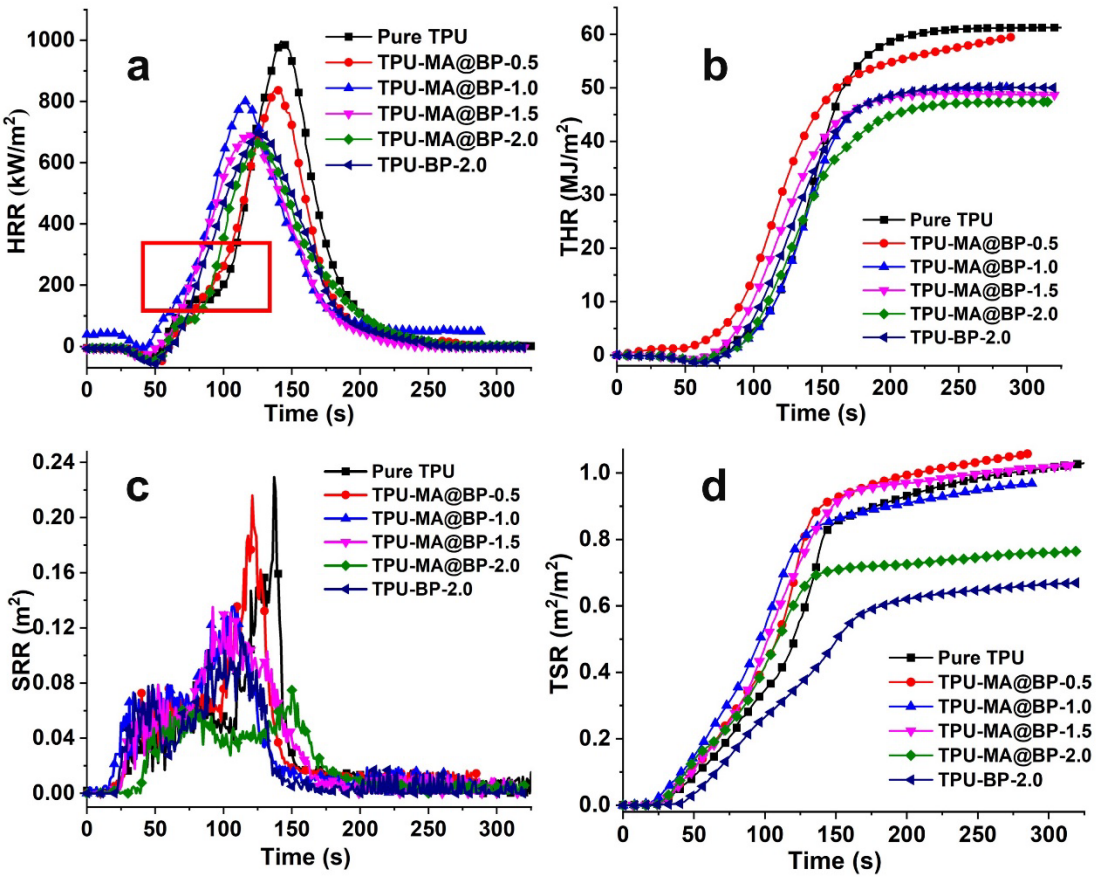

Figure 5 HRR (a), THR (b), SPR (c) and TSR (d) curves of pure TPU and its composites

Table 2 cone calorimeter data of of pure TPU and its composites

	PHRR (kW/m²)	THR (MJ/m²)	SPR (m²/s)	TSR (m²/m²)	Char residue (wt%)
Pure TPU	982.1	61.4	0.230	1.030	2.77
TPU-MA@BP-0.5	836.0	59.4	0.216	1.056	5.38
TPU-MA@BP-1.0	800.5	50.0	0.134	0.971	5.15
TPU-MA@BP-1.5	683.5	48.7	0.135	1.019	6.76
TPU-MA@BP-2.0	660.6	47.4	0.074	0.760	9.28
TPU-BP-2.0	703.0	50.0	0.103	0.662	10.93

The smoke production process is also detected by an infrared laser sensor. An extremely pointed peak is presented in the SPR curve of pure TPU, demonstrating a

drastic and rapid formation of smoke particles (Figure 5c). The addition of pure BP nanosheets effectively decreases the SPR of TPU composite, from 0.230 m/s^2 (pure TPU) to 0.103 m/s^2. As reported in our previous literature, pure BP nanosheets will significantly promote smoke formation during combustion[35]. The obvious distinction may be due to the different char-forming abilities of polyester and polyether TPU. In addition, 2.0wt% MA@BP nanosheets present a more significant suppression effect, with an SPR of 0.074 m^2/s, corresponding to a reduction of 67.8%. Even though the lowest decrease in SPR is presented in TPU-MA@BP-2.0, pure BP nanosheets impart the largest reduction in TSR values. It is found that the TSR of TPU-BP-2.0 is low to 0.662 m^2/m^2, presenting a decrease of up to 35.7% compared with pure TPU (Figure 5d and Table 2). These results demonstrate that pure BP nanosheets are more efficient than MA@BP nanosheets, in the ultimate formation of smoke particles. It may be due to the pyrolysis products of BP nanosheets, including metaphosphoric acid and phosphorus-containing radicals, which can react with polymer resin to form a protective char layer, thus decreasing the total amount of smoke particles[36]. Obviously, the existence of melamine reduces the corresponding ratio of BP nanosheets in MA@BP nanosheets. Besides, attributed to the melamine, MA@BP nanosheets will delay the production rate of smoke particles.

In addition to combustion heat and smoke particles, CO and CO_2 release behaviors are also recorded (Figure 6). Compared to TPU-BP and TPU-MA@BP composites, pure TPU has an extremely high release rate of CO near 0.196 mg/m^2, demonstrating a huge gas toxicity (Figure 6a). The addition of pure BP and MA@BP nanosheets all decrease the CO release rate. 2.0wt% pure BP decreases the CO release rate of TPU resin to 0.099 mg/m^2 from 0.196 mg/m^2, with a reduction of 50.5%. Besides, the release rates of CO gas are gradually decreased to 0.139 mg/m^2, 0.118 mg/m^2, and 0.070 mg/m^2, with the addition of 0.5wt%, 1.0wt%, and 1.5wt% MA@BP, respectively. It is found that the release peaks are gradually lower and thus the release peak in TPU-MA@BP-2.0 is disappeared. As a result, the total CO release of TPU-MA@BP-2.0 is significantly decreased to 2.40 $(mg/m^3)*s$ from 10.12 $(mg/m^3)*s$ (pure TPU), corresponding to a reduction of 76.3% (Figure 6c). The CO_2 is the main product of TPU combustion and

its release behavior is similar to combustion heat. In comparison with the release rate of pure TPU (0.711%), the incorporation of 2.0wt% pure BP (~0.535%) and MA@BP nanosheets (~0.527%) leads to very approximate CO_2 release rates in TPU composites (Figure 6b). However, pure BP nanosheets promote the release of CO_2 in the second step and more CO_2 is released during TPU-BP-2.0 combustion. As a result, the total CO_2 release of TPU-MA@BP-2.0 is 35.3 %*s, much lower than 45.6 %*s (pure TPU) and 39.5 %*s (TPU-BP-2.0) (Figure 6d).

Based on this atomic (carbon) conservation law, we reasonably put forward a formula

$$C_{total} = C_{CO2} + C_{CO} + C_{char} + C_{smoke} \quad (4)$$

where C_{total} is the total carbon content in TPU composite, C_{CO2}, C_{CO}, C_{char}, and C_{smoke} are the corresponding carbon content in CO_2, CO, char residue, and smoke. It is found that MA@BP nanosheets are more efficient in reducing CO_2 and CO, while pure BP nanosheets have a better suppression effect in smoke and char residue (Table 2). The heat release is tightly related to the CO_2 and CO produced by TPU combustion. Therefore, it is logical that TPU-MA@BP-2.0 has a lower THR. We are very curious about the atomic (carbon) conservation during combustion. The decreases in C_{CO2}, C_{CO}, and C_{smoke} are not supported by the increase in C_{char} (Table 2). The quantitative relationship needs a deeper investigation provided by a new device or technology. In addition, a conclusion can be drawn that MA@BP nanosheets can effectively decrease the release of heat, CO_2, and toxic CO, while pure BP nanosheets are more efficient in suppressing the formation of smoke particles. In other words, MA@BP nanosheets present a comprehensive flame retardancy effect, compared with pure BP nanosheets.

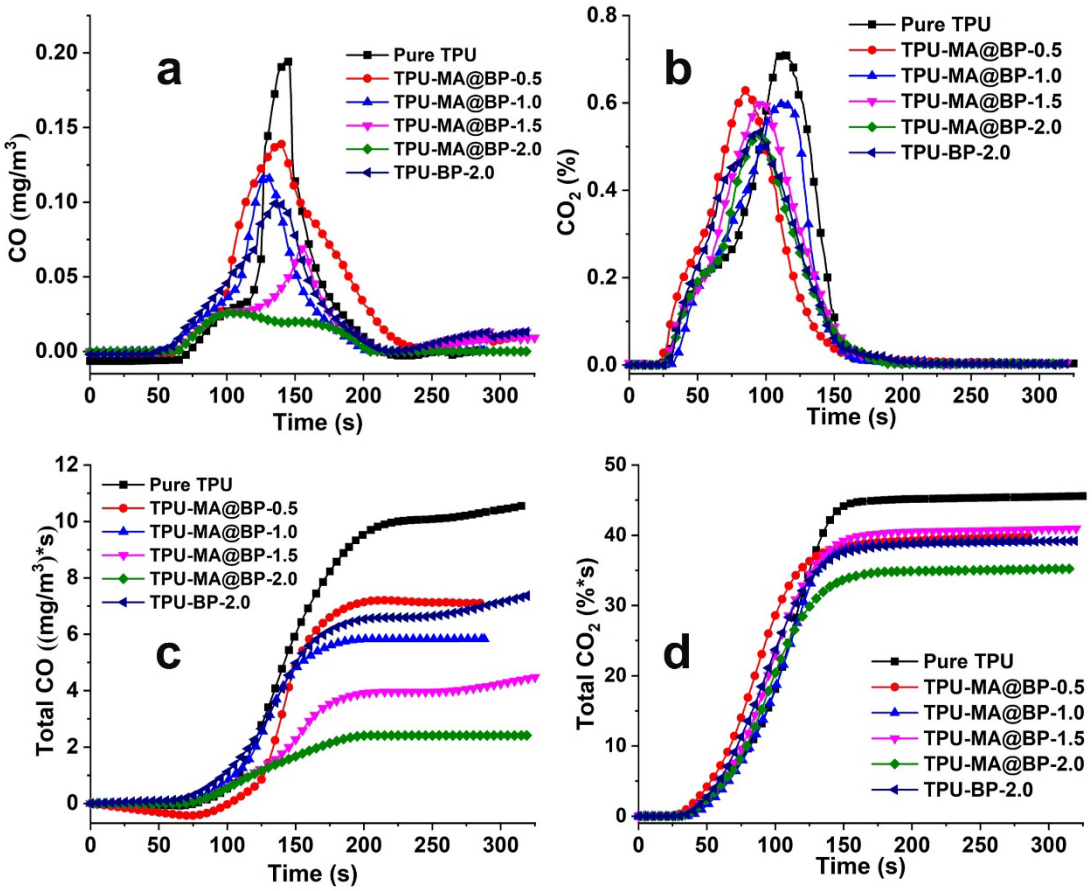

Figure 6 Release rate (a and b) and total release (c and d) curves of CO and CO_2 gases.

3.4 Flame retardancy mechanism

In order to reveal the flame retardancy mechanism of MA@BP nanosheets, the pyrolysis products of TPU composites in gaseous and condensed phases will be investigated. After being pyrolyzed under a nitrogen atmosphere, the pyrolysis products are investigated with FTIR spectrum, i.e., TG-FTIR test. The 3D time-wavenumber-absorbance spectra of pure TPU and TPU-MA@BP-2.0 are presented in Figures 7a and 7b. It is found that the characteristic peak near 1746 and 2360 cm^{-1} demonstrate an obvious difference in pure TPU and TPU-MA@BP-2.0, indicating the change in the thermal pyrolysis process[37]. The FTIR spectra of pure TPU and TPU-MA@BP-2.0 are presented in Figure 7c_1, obtained in the strongest signal location. As presented, the characteristic peaks in pyrolysis products of pure TPU and TPU-MA@BP-2.0 are coincident. This result illustrates that incorporated MA@BP nanosheets are not able to change the kind of pyrolysis products. Characteristic peaks near 2975, 2360, 1746, and

1146 cm^{-1} are assigned to hydrocarbons, CO_2, carbonyl, and others [38]. After being divided by test mass, the signal intensity versus time curves of total and characteristic peaks are shown in Figures 7c_2-c_6. Unexpectedly, the signal intensity of total pyrolysis products is enhanced by the addition of MA@BP nanosheets. Meanwhile, it is found that incorporating MA@BP nanosheets will reduce the signal intensity of hydrocarbons, carbonyl, and ethers. However, the signal intensity of CO_2 is increased, confirming that MA@BP nanosheets will promote the formation of CO_2 gas.

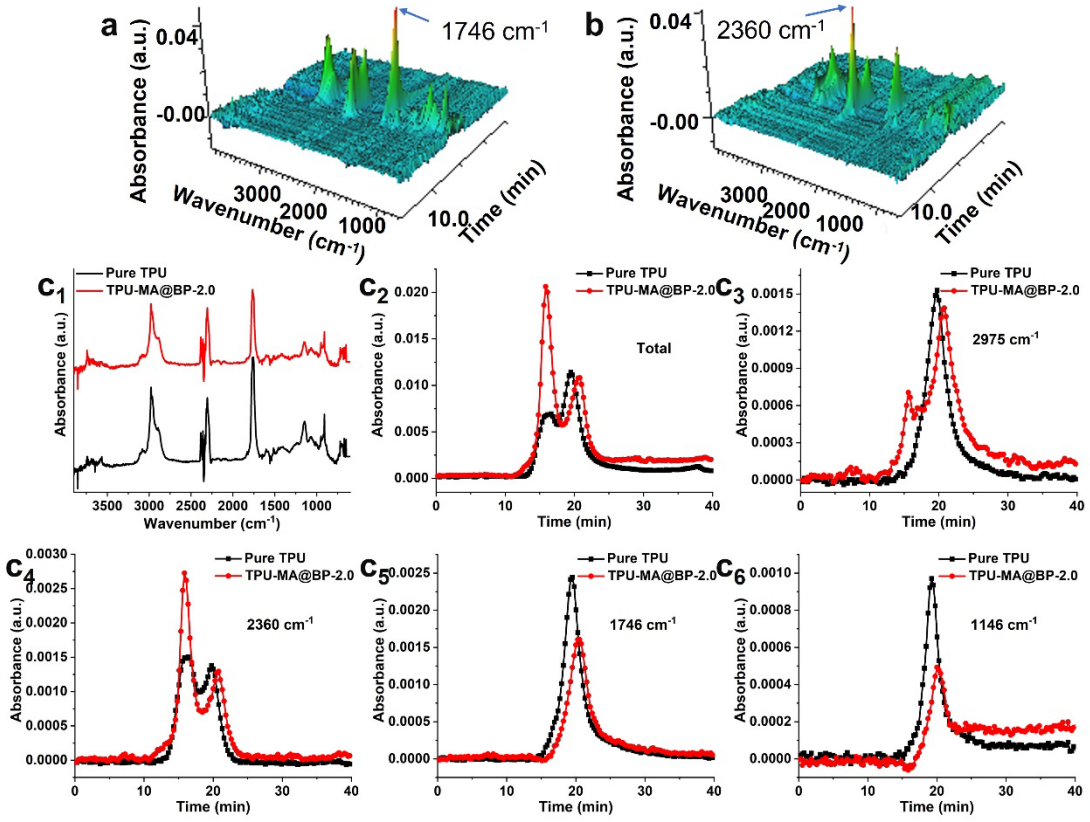

Figure 7 3D-diagram of TGA-IR spectra of pure TPU (a) and TPU-MA@BP-2.0 (b); (c_1) FTIR spectra of pure TPU and TPU-MA@BP-2.0 at maximum intensity; (c_2-c_6) Absorption intensity of total and characteristic products of pure TPU and TPU-MA@BP-2.0.

After the cone calorimeter test, char residues of pure TPU, TPU-MA@BP-2.0, and TPU-BP-2.0 present different physical morphology. Compared to the thin structure in the char residue of pure TPU, obviously more and thicker char residues are left in TPU-MA@BP-2.0 and TPU-BP-2.0 (Figures 8a_1, b_1, and c_1). Interestingly, a lot of holes are formed on the surface of the char layer of TPU-MA@BP-2.0. However, there are no

holes existed in TPU-BP-2.0. Meanwhile, some fissure, which may be due to the melt contraction of TPU resin, is produced. These holes contribute to the thermal pyrolysis of melamine. Compared to the dense structure of the char residue of pure TPU, micro-voids and concave-down morphology presented in the char residue of TPU-MA@BP-2.0 also indicate the distinguishing flame retardant mechanism. The graphitization degree of char residue from pure TPU, TPU-MA@BP-2.0, and TPU-BP-2.0 is studied by the Raman spectrum (Figures $8a_2$, $8b_2$, and $8c_2$). The characteristic peaks near 1360 cm^{-1} and 1590 cm^{-1} are assigned to G-band and D-band, which are very sensitive to order structure, defects, and disorders[39]. The Raman intensity ratio of G-band to D-band (I_G/I_D) is regarded as a critical parameter to determine the graphitization degree. The addition of MA@BP and pure BP nanosheets increases the I_G/I_D value to 0.333 and 0.305 from 0.288 (pure TPU). The higher I_G/I_D indicates that char residue from TPU-MA@BP-2.0 combustion has a higher graphitization degree with a thermally stable structure. Besides, the modification of melamine promotes the effect of BP nanosheets in the increase of graphitization degree. Based on the above results, a synergistic flame retardancy mechanism in the gaseous and condensed phases is put forward (Figure 8d). According to the decomposition temperature, melamine will be pyrolyzed into NH_3 or nitrogen to decrease the combustible concentration in the gaseous phase. Then, phosphorus-containing acids and free radicals pyrolyzed from BP nanosheets will react with TPU resin and chain-growth free radicals, respectively, to form condensed char and quench the chain growth.

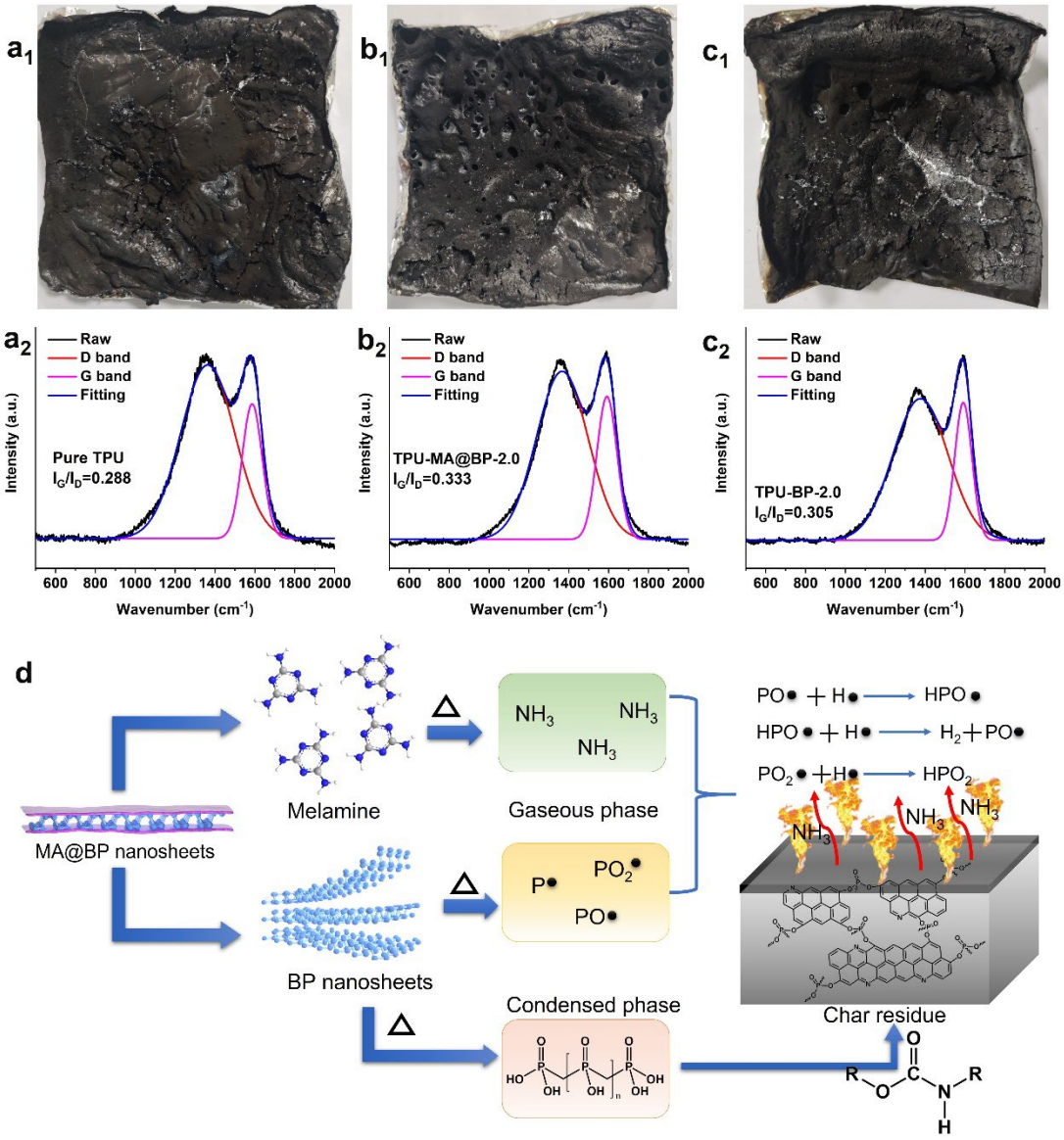

Figure 8 Digital photo and Raman spectra of pure TPU (a),TPU-MA@BP-2.0 (b), and TPU-BP-2.0 (c); (d) schematic for the flame retardancy mechanism of MA@BP nanosheets.

3.5 Photo-thermal conversion performance

As reported by previous literature, due to a bandgap structure of 0.3-2.0 eV, BP nanosheets have presented a well solar absorption and conversion capability[40]. Therefore, it is speculated that incorporated MA@BP nanosheets will impart TPU matrix with well photo-thermal conversion ability. Pure TPU has high absorption in UV region and high transmittance in the visible and NIR region (Figure 9a). Obviously, the

addition of MA@BP nanosheets increases the solar absorption to ~90%. Based on formula 5[41],

$$a = \int_{\lambda min}^{\lambda max} I(\lambda)\alpha(\lambda)d\lambda / \int_{\lambda min}^{\lambda max} I(\lambda)d\lambda \quad (5)$$

the overall solar absorption of TPU-MA@BP-2.0 can be calculated, where α is the solar absorptivity, I(λ) is solar intensity, λ is the wavelength (μm), λ_{min} and λ_{max} are 0.3 μm and 2.5 μm, respectively. It is found that the overall solar absorptivity of TPU-MA@BP-2.0 composite is up to 91.0%. After being illuminated by 1.0 kW/m^2 simulated solar, the surface temperatures of pure TPU and TPU-MA@BP-2.0 is recorded by a thermocouple (Figure 9b). The surface equilibrium temperature in pure TPU is ~57.6 ºC, attributed to the heating effect of NIR light. TPU-MA@BP-2.0 presents a rapid temperature increase, achieving ~71 ºC at 130s, and finally keeps at an equilibrium temperature of ~80 ºC. Meanwhile, the average surface temperature of near 79.1 ºC confirms the high repeatability and robustness (Figure 9c). The thermal imaging is also provided with an infrared thermal imager. It is presented that the surface temperature is slowly increased in pure TPU and achieves 59.5 ºC at 600s (Figures 9d$_1$ and S3a). The addition of MA@BP nanosheets effectively increases the heating rate and equilibrium temperature. TPU-MA@BP-2.0 achieved 64.2 ºC at 60s and an equilibrium temperature of 92.0 ºC (Figures 9d$_2$ and S3b). It is found that the temperature difference existed between the thermocouple and infrared thermal imager, attributed to the different test methods.

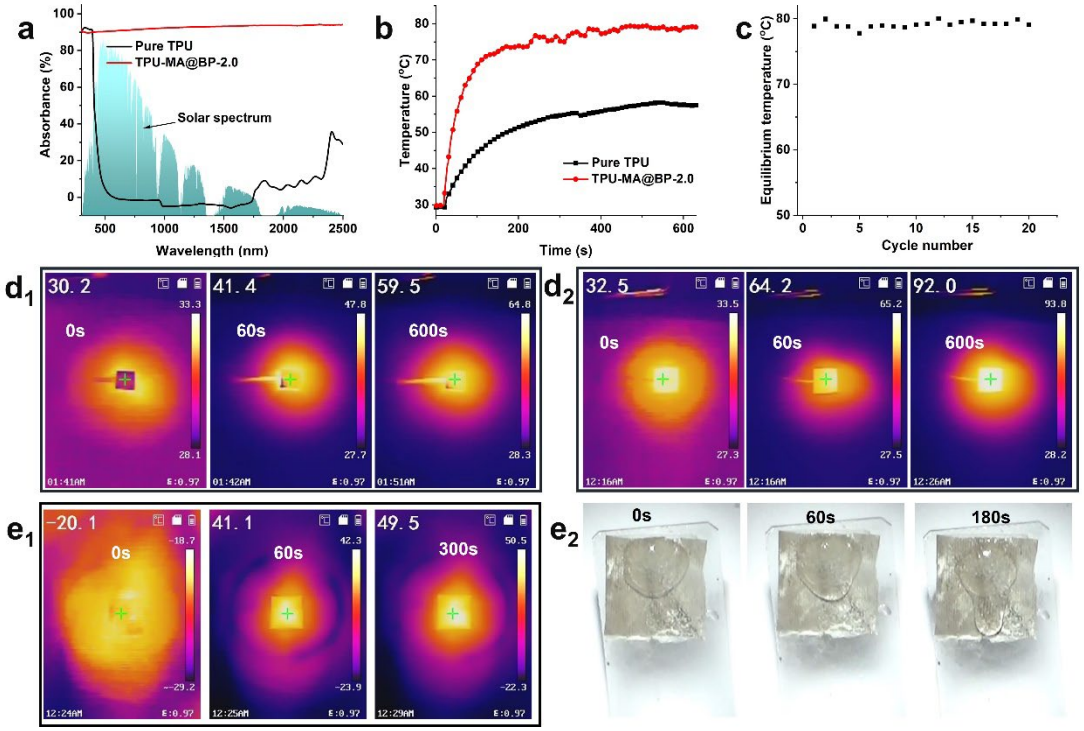

Figure 9 Solar absorption curves (a) and temperature curves under simulated sunlight of 1.0 kW/m^2 (b) of pure TPU and TPU-MA@BP-2.0; (c) The equilibrium temperature of TPU-MA@BP-2.0 in repeated 20 times; thermal imagery of pure TPU (d_1) and TPU-MA@BP-2.0 (d_2) under simulated sunlight of 1.0 kW/m^2; Thermal imagery of TPU-MA@BP-2.0 (e_1) under -20 °C and simulated sunlight of 1.0 kW/m^2; (e_2) Melting process of ice onto the surface of TPU-MA@BP-2.0 under -20 °C and simulated sunlight of 1.0 kW/m^2.

Due to the desirable photo-thermal conversion effect, it is believed that TPU-MA@BP-2.0 can absorb and convert solar energy into heat, even in cold environments. To demonstrate this anticipation, a home-made device is developed to simulate the cold environment (-20 °C). With simulated solar of 1.0 kW/m^2, pure TPU still obtains a surface temperature of 9.2 °C (Figure S4a). Compared to pure TPU, TPU-MA@BP-2.0 has a significant photo-thermal conversion effect. During 60s, the surface temperature of TPU-MA@BP-2.0 rapidly increases to 41.1 °C, from -20.1 °C (Figures 9e_1 and S4b). Meanwhile, the equilibrium temperature is up to 49.5 °C. It is found that, during this illumination process, the environment temperature remains at -20 °C. These results indicate that TPU-MA@BP-2.0 can effectively convert solar energy to heat, even under

a cold environment of -20 °C. A simple test is performed to investigate the photo-thermal conversion of TPU-MA@BP-2.0 in the de-icing performance (Figure 9e$_2$ and S5). An irregular ice is frozen onto the surface of TPU-MA@BP-2.0, in an environment of -20 °C. With simulated sunlight of 1.0 kW/m^2, TPU-MA@BP-2.0 produces a lot of heat to promote ice melting. Therefore, water flow can be observed at 90s and is gradually increased with increasing time. The ice-melting phenomenon confirms the huge potential of TPU-MA@BP-2.0 as a de-icing material.

4. Conclusion

Inspired by the microstructure in spider silk, the hydrogen bond interactions are employed to drive the self-assembly process of melamine onto the surface of BP nanosheets, thus preparing P/N-containing advance nano flame retardant, without the consumption of any organic solvent. The first-principles calculations confirm that melamine can spontaneously adsorb onto the surface of BP nanosheets and enhance the interfacial interactions between BP nanosheets and TPU resin. As confirmed by the TEM and SEM photographs, melamine is uniformly distributed onto the surface of BP nanosheets. Compared to pure BP nanosheets, MA@BP nanosheets present more efficient suppression effects in heat release and toxic CO production. The addition of 2.0 wt% MA@BP nanosheets decreases PHRR and THR values to 660.6 kW/m^2 and 47.4 MJ/m^2 from 982.1 kW/m^2 and 61.4 MJ/m^2 (pure TPU). Meanwhile, with the reduction of 76.3% in total release, the release peak of toxic CO is not presented. Based on the TG-IR spectrum and morphologies of char residue, a synergistic flame retardancy mechanism in the gaseous and condensed phase is put forward. BP nanosheets first react with TPU resin to form condensed char in the condensed phase and then melamine will be pyrolyzed into NH_3 or nitrogen to decrease the combustible concentration in the gaseous phase. Besides, due to the photo-thermal conversion effect of BP nanosheets, TPU-MA@BP-2.0 presents an equilibrium temperature of ~80 °C under simulated sunlight of 1.0 kW/m^2. Along with a high photo-thermal conversion performance in an environment of low temperature, the melting process is significantly

promoted by the solar harvest. The solve-free and hydrogen-bond assembly method overcomes the lack problem of functional groups onto the surface of BP nanosheets, thus providing a new approach to develop the flame retardancy effect of BP nanosheets.

Acknowledgements

The authors acknowledge financial support from the National Key Research and Development Program of China (2022YFC3003100), the Hong Kong Environment and Conservation Fund (ECF 107/2020, P0034081), the National Natural Science Foundation of China (22205228), and the Fellowship of China Postdoctoral Science Foundation (2021M703054 and 2022T150613).

Reference:

[1] T. Yang, J. Hu, P. Wang, M. Edeleva, L. Cardon, J. Zhang, Two-step approach based on fused filament fabrication for high performance graphene/thermoplastic polyurethane composite with segregated structure, Compos. Part A-Appl. S., 174 (2023) 107719.

[2] L. Wan, C. Deng, H. Chen, Z.Y. Zhao, S.C. Huang, W.C. Wei, A.H. Yang, H.B. Zhao, Y.Z. Wang, Flame-retarded thermoplastic polyurethane elastomer: From organic materials to nanocomposites and new prospects, Chem. Eng. J., 417 (2021) 129314.

[3] H.Y. Ren, K.L. Qing, Y. Chen, Y.J. Lin, X. Duan, Smoke suppressant in flame retarded thermoplastic polyurethane composites: Synergistic effect and mechanism study, Nano Res., 14 (2021) 3926-3934.

[4] W. Cai, B.-B. Wang, X. Wang, Y.-L. Zhu, Z.-X. Li, Z.-M. Xu, L. Song, W.-Z. Hu, Y. Hu, Recent progress in two-dimensional nanomaterials following graphene for improving fire safety of polymer (nano) composites, Chinese J. Polym. Sci., 39 (2021) 935-956.

[5] G.B. Huang, W. Chen, T. Wu, H.C. Guo, C.Y. Fu, Y.J. Xue, K. Wang, P.A. Song, Multifunctional graphene-based nano-additives toward high-performance polymer nanocomposites with enhanced mechanical, thermal, flame retardancy and smoke

595 suppressive properties, Chem. Eng. J., 410 (2021) 127590.
596 [6] H. Lim, B.L. Suh, M.J. Kim, H. Yun, J. Kim, B.J. Kim, S.G. Jang, High-performance,
597 recyclable ultrafiltration membranes from P4VP-assisted dispersion of flame-resistive
598 boron nitride nanotubes, J. Membrane Sci., 551 (2018) 172-179.
599 [7] W.H. Chen, P.J. Liu, Y. Liu, Z.X. Liu, Recent advances in Two-dimensional Ti_3C_2Tx
600 MXene for flame retardant polymer materials, Chem. Eng. J., 446 (2022) 137239.
601 [8] W. Wang, C. Wang, A. Yuen, Ao Li, B. Lin, Y. Yuan, C. Ma, Y. Han, G. Yeoh, 3D
602 MXene frameworks for flame retardant hydrophobic polymer nanocomposites,
603 Compos. Part A: Appl. S., 173 (2023) 107673
604 [9] Y. Hou, Z. Xu, R. An, H. Zheng, W. Hu, K. Zhou, Recent progress in black
605 phosphorus nanosheets for improving the fire safety of polymer nanocomposites,
606 Compos. Part B: Eng. 249 (2023) 110404.
607 [10] Z. Qian, B. Zou, Y. Xiao, S. Qiu, Z. Xu, Y. Yang, G. Jiang, Z. Zhang, L. Song, Y.
608 Hu, Targeted modification of black phosphorus by MIL-53(Al) inspired by “Cannikin's
609 Law” to achieve high thermal stability of flame retardant polycarbonate at ultra-low
610 additions, Compos. Part B: Eng. 238 (2022) 109943.
611 [11] W. Cai, T. Cai, L. He, F. Chu, X. Mu, L. Han, Y. Hu, B. Wang, W. Hu, Natural
612 antioxidant functionalization for fabricating ambient-stable black phosphorus
613 nanosheets toward enhancing flame retardancy and toxic gases suppression of
614 polyurethane, J. Hazard. Mater., 387 (2020) 121971.
615 [12] Q. Liu, D. Feng, W.B. Zhao, D.L. Xie, Y. Mei, A green, effective, and synergistic
616 flame retardant for poly (ethylene-co-vinyl acetate) resin, Polym. Degrad. Stabil., 206
617 (2022) 110201.
618 [13] S. Shang, B. Yuan, Y. Sun, G. Chen, C. Huang, B. Yu, S. He, H. Dai, X. Chen,
619 Facile preparation of layered melamine-phytate flame retardant via supramolecular
620 self-assembly technology, J. Colloid Interf. Sci., 553 (2019) 364-371.
621 [14] Z.M. Zhu, P.L. Lin, H. Wang, L.X. Wang, B. Yu, F.H. Yang, A facile one-step
622 synthesis of highly efficient melamine salt reactive flame retardant for epoxy resin, J.
623 Mater. Sci., 55 (2020) 12836-12847.
624 [15] H.L. Li, Y. Li, B.L. Li, Y. Dai, X. Chen, Melamine-induced novel MSONs

heterostructured framework: Controlled-switching between MOF and SOF via a self-assembling approach for rapid uranium sequestration, Chem. Eng. J., 379 (2020) 122279.
[16] W. Huang, D. Restrepo, J.Y. Jung, F.Y. Su, Z. Liu, R.O. Ritchie, J. McKittrick, P. Zavattieri, D. Kisailus, Multiscale Toughening Mechanisms in Biological Materials and Bioinspired Designs, Adv. Mater., 31 (2019) e1901561.
[17] P. Song, Z. Xu, Q. Guo, Bioinspired Strategy to Reinforce PVA with Improved Toughness and Thermal Properties via Hydrogen-Bond Self-Assembly, ACS Macro Lett., 2 (2013) 1100-1104.
[18] S. Ling, W. Chen, Y. Fan, K. Zheng, K. Jin, H. Yu, M.J. Buehler, D.L. Kaplan, Biopolymer nanofibrils: structure, modeling, preparation, and applications, Prog. Polym. Sci., 85 (2018) 1-56.
[19] P.G. Song, Z.G. Xu, Y.P. Wu, Q.F. Cheng, Q.P. Guo, H. Wang, Super-tough artificial nacre based on graphene oxide via synergistic interface interactions of pi-pi stacking and hydrogen bonding, Carbon 111 (2017) 807-812.
[20] P. Song, H. Wang, High-Performance Polymeric Materials through Hydrogen-Bond Cross-Linking, Adv. Mater., 32 (2020) e1901244.
[21] W. Cai, X.W. Mu, Y. Pan, Z.X. Li, J.L. Wang, X. Zhou, W.W. Guo, W.Z. Hu, L. Song, Y. Hu, Black Phosphorous Nanosheets: A Novel Solar Vapor Generator, Sol. Rrl 4 (2020).
[22] S. Wu, K.S. Hui, K.N. Hui, 2D Black Phosphorus: from Preparation to Applications for Electrochemical Energy Storage, Adv. Sci., 5 (2018) 1700491.
[23] T. Liu, Y. Liu, M. Chen, X. Guo, S. Tang, R. Zhang, Z. Xie, J. Wang, A. Gu, S.J.A.F.M. Lin, Fluorinated black phosphorene nanosheets with robust ambient stability for efficient and stable perovskite solar cells, Adv. Funct. Mater., 32 (2022) 2106779.
[24] J. Huang, B. He, Z. Zhang, Y. Li, M. Kang, Y. Wang, K. Li, D. Wang, B.Z. Tang, Aggregation-Induced Emission Luminogens Married to 2D Black Phosphorus Nanosheets for Highly Efficient Multimodal Theranostics, Adv. Mater., 32 (2020) e2003382.
[25] G. Tang, H. Jiang, Y. Yang, D. Chen, C. Liu, P. Zhang, L. Zhou, X. Huang, H.

Zhang, X.J.J.o.P.R. Liu, Preparation of melamine–formaldehyde resin-microencapsulated ammonium polyphosphate and its application in flame retardant rigid polyurethane foam composites, J. Polym. Res., 27 (2020) 1-14.
[26] H.B. Ribeiro, M.A. Pimenta, C.J. de Matos, R.L. Moreira, A.S. Rodin, J.D. Zapata, E.A. de Souza, A.H. Castro Neto, Unusual angular dependence of the Raman response in black phosphorus, ACS Nano 9 (2015) 4270-4276.
[27] W.L. Lu, H.Y. Nan, J.H. Hong, Y.M. Chen, C. Zhu, Z. Liang, X.Y. Ma, Z.H. Ni, C.H. Jin, Z. Zhang, Plasma-assisted fabrication of monolayer phosphorene and its Raman characterization, Nano Res., 7 (2014) 853-859.
[28] G. Zhao, T. Wang, Y. Shao, Y. Wu, B. Huang, X. Hao, A Novel Mild Phase-Transition to Prepare Black Phosphorus Nanosheets with Excellent Energy Applications, Small 13 (2017) 1602243.
[29] F.B. Ajdari, E. Kowsari, A. Ehsani, L. Chepyga, M. Schirowski, S. Jager, O. Kasian, F. Hauke, T. Ameri, Melamine-functionalized graphene oxide: Synthesis, characterization and considering as pseudocapacitor electrode material with intermixed POAP polymer, Appl. Surf. Sci., 459 (2018) 874-883.
[30] A. Ambrosi, Z. Sofer, M. Pumera, Electrochemical Exfoliation of Layered Black Phosphorus into Phosphorene, Angew Chem. Int. Edit., 56 (2017) 10443-10445.
[31] C. Jiao, H. Wang, S. Li, X. Chen, Fire hazard reduction of hollow glass microspheres in thermoplastic polyurethane composites, J. Hazard. Mater., 332 (2017) 176-184.
[32] Y.F. Quan, Z.R. Zhang, R.N. Tanchak, Q.S. Wang, A review on cone calorimeter for assessment of flame-retarded polymer composites, J. Therm. Anal. Calorim., 147 (2022) 10209-10234.
[33] G.B. Huang, P.A. Song, L.N. Liu, D.M. Han, C.H. Ge, R.R. Li, Q.P. Guo, Fabrication of multifunctional graphene decorated with bromine and nano-Sb_2O_3 towards high-performance polymer nanocomposites, Carbon 98 (2016) 689-701.
[34] W. Cai, X. Feng, B. Wang, W. Hu, B. Yuan, N. Hong, Y.J.C.E.J. Hu, A novel strategy to simultaneously electrochemically prepare and functionalize graphene with a multifunctional flame retardant, Chem. Eng. J., 316 (2017) 514-524.

[35] W. Cai, Z. Li, X. Mu, L. He, X. Zhou, W. Guo, L. Song, Y.J.J.o.H.M. Hu, Barrier function of graphene for suppressing the smoke toxicity of polymer/black phosphorous nanocomposites with mechanism change, J. Hazard. Mater., 404 (2021) 124106.
[36] S.H. Yin, X.L. Ren, R.Z. Zheng, Y.X. Li, J.P. Zhao, D.L. Xie, Y. Mei, Improving fire safety and mechanical properties of waterborne polyurethane by montmorillonite-passivated black phosphorus, Chem. Eng. J., 464 (2023) 142683.
[37] J.L. Wang, C. Ma, X.W. Mu, X. Zhou, L.X. He, Y.L. Xiao, L. Song, Y. Hu, Designing 3D ternary-structure based on SnO_2 nanoparticles anchored hollow polypyrrole microspheres interconnected with N, S co-doped graphene towards high-performance polymer composite, Chem. Eng. J., 402 (2020) 126221.
[38] S.Y. Chan, L. Si, K.I. Lee, P.F. Ng, L. Chen, B. Yu, Y. Hu, R.K. Yuen, J.H. Xin, B.J.C. Fei, A novel boron–nitrogen intumescent flame retardant coating on cotton with improved washing durability, Cellulose 25 (2018) 843-857.
[39] Y.M. Xu, X. Chen, L. Wang, K. Bei, J.L. Wang, I.M. Chou, Z.Y. Pan, Progress of Raman spectroscopic investigations on the structure and properties of coal, J. Raman Spectrosc., 51 (2020) 1874-1884.
[40] X. Zhu, T. Zhang, Z. Sun, H. Chen, J. Guan, X. Chen, H. Ji, P. Du, S. Yang, Black Phosphorus Revisited: A Missing Metal-Free Elemental Photocatalyst for Visible Light Hydrogen Evolution, Adv. Mater., 29 (2017) 1605776.
[41] M. Li, Z. Yan, D. Fan, Flexible Radiative Cooling Textiles Based on Composite Nanoporous Fibers for Personal Thermal Management, ACS Appl. Mater. Inter., 15 (2023) 17848-17857.